Proceedings of the Sixth International Conference on
Railway Technology: Research, Development and Maintenance
Edited by: J. Pombo
Civil-Comp Conferences, Volume 7, Paper 16.3
Civil-Comp Press, Edinburgh, United Kingdom, 2024
ISSN: 2753-3239, doi: 10.4203/ccc.7.16.3

Identifying the Separate Contributions of Electromagnetic and Wave-Induced Instability Mechanisms to the Overall Dynamic Instability in Hyperloop and Maglev Systems

A. B. Fărăgău, A. V. Metrikine, K. N. van Dalen, J. Paul and R. J. Van Leijden

Faculty of Civil Engineering and Geosciences, Delft University of Technology, Netherlands

Abstract

The Hyperloop, a developing transportation system, reduces air resistance by housing the vehicle within a depressurized tube and eliminates contact friction by using an electro-magnetic suspension/levitation system. Maintaining system stability poses a challenge due to the exceptionally high target velocities. Consequently, it is important to know apriori the velocity regimes in which the system can be unstable. The authors have recently investigated this aspect by, unlike previous studies, properly accounting for the frequency and velocity dependent reaction force provided by the infinite guideway. Furthermore, that study focused on the interplay between two fundamentally different instability sources, namely (i) the electro-magnetic suspension, and (ii) wave-induced instability, showing that stability domains drastically change above a certain vehicle velocity. The current study presents a methodology to distinguish the contribution of each instability mechanism to the overall system stability, and demon-

strates that the wave-induced instability mechanism is causing the drastic stability change at large vehicle velocities. This investigation offers physical insight into the mechanisms that can cause instability in the Maglev/Hyperloop systems, and can help engineers that develop this novel transportation system to avoid excessive vibrations and, in extreme cases, derailment.

Keywords: Hyperloop, magnetically-levitated vehicles, Maglev, dynamic stability, anomalous Doppler waves, moving-load dynamics.

1 Introduction

Hyperloop is an innovative transportation system that is currently under development. It minimizes air resistance by enclosing the vehicle in a de-pressurized tube and eliminates wheel-rail contact friction through the use of an electromagnetic suspension/levitation, similar to Maglev trains. This design can potentially achieve much higher velocities compared to traditional railways, positioning the Hyperloop as an environmentally friendly alternative to air transportation.

Some challenges encountered by the Hyperloop system have already been explored within the context of high-speed railways (e.g., vehicle-structure-soil interaction at large velocities [1–3], fatigue/degradation critical locations in the structure such as transition zones [4–8], influence of guideway periodicity on the system response [9] and system stability [10–12], etc.) and of magnetic levitation (Maglev) transportation systems [13] (e.g., levitation and propulsion design [14, 15], electro-dynamic instability [14], electro-magnetic instability [16, 17], aerodynamic instability [17, 18], parametric instability [19], etc.).

However, due to the substantially higher target velocities, it is anticipated that new hurdles will arise [20, 21]. One such challenge involves ensuring the dynamic stability of the system at these elevated velocities, aiming to prevent excessive amplifications of the response. It is widely recognized that when a vehicle travels on an elastic guideway, its vibrations can become unstable once it surpasses a certain critical velocity [22]. Metrikin [23] demonstrated that instability arises when the energy associated with the radiation of anomalous Doppler waves, which feed back energy into the vehicle's vibration, exceeds that of normal Doppler waves. Identifying the velocity ranges in which the Hyperloop system may become unstable (i.e., determining critical velocities [2, 22, 24–30]) is crucial for its design and practical implementation.

The authors have previously investigated the interplay between the electro-magnetic and wave-induced instability mechanisms [31], and showed that the stability space changes significantly above a certain velocity. In other words, the control strategy can ensure the overall system stability only for a very limited range of its gains. The cause for this drastic change was attributed to the wave-induced instability mechanism [31]. The current study presents a methodology to distinguish the contribution of each instability mechanism to the overall system stability. More specifically, the

energy variation of the vehicle is divided in two components corresponding to (i) energy input by the electro-magnetic suspension and (ii) energy input by the guideway. While identifying unstable velocity regimes is practical for Hyperloop design, the ability to discern which mechanism causes system instability for a certain parameter combination is valuable can be crucial for efficient mitigation.

2 Model formulation

In this study, the system under consideration comprises an infinite Euler-Bernoulli beam characterized by mass per unit length ρ and bending stiffness EI. The beam is continuously supported by distributed springs (k_d) and dashpots (c_d). A vehicle with mass M and velocity v acts upon the guideway. The connection between the vehicle and the guideway involves a nonlinear electromagnetic force F, akin to the electromagnetic suspension utilized in Maglev trains, operating solely in attraction [18]. To facilitate the chosen solution approach, it is advantageous to express the governing equations in the reference frame moving with the vehicle, denoted by $\xi = x - v\bar{t}$ and $t = \bar{t}$, where $(x, \bar{t})$ and (ξ, t) represent the spatial and temporal coordinates in the stationary and moving reference frames, respectively. The system configuration is illustrated in Fig. 1, with its governing equations detailed in [18] and presented in the following:

$$EIw'''' + \rho\big(\ddot{w} - 2v\dot{w}' + v^2w''\big) + c_\mathrm{d}\big(\dot{w} - vw'\big) + k_\mathrm{d}w = -F(t)\delta(\xi), \tag{1}$$

$$M\ddot{u} = F(t) - Mg, \tag{2}$$

$$F(t) = C\frac{I^2}{\big(w_0 - u\big)^2}, \tag{3}$$

$$\dot{I} = \frac{w_0 - u}{2C}\Big(U - IR + 2C\frac{I}{\big(w_0 - u\big)^2}(\dot{w}_0 - \dot{u})\Big), \tag{4}$$

$$U = K_\mathrm{p}\big(w_0 - u - \Delta^\mathrm{ss}\big) + K_\mathrm{d}\big(\dot{w}_0 - \dot{u}\big) + U^\mathrm{ss}, \tag{5}$$

where primes and overdots denote partial derivatives in space ξ and time t, respectively, g is the gravitational acceleration, δ represents the Dirac delta function, u is the mass displacement, and $w_0 = w(\xi = 0)$ is the beam displacement under the moving mass. The electro-magnetic force F depends on the current intensity I and on the air-gap $\Delta = w_0 - u$, while C is a constant that depends on the electro-magnet properties [18]. Eq. (4) is a nonlinear differential equation governing the current intensity where U is the voltage and R is the circuit resistance.

In the absence of a control strategy, the formulated system exhibits inherent instability, even in the absence of vehicle horizontal motion. Consequently, a control strategy is implemented on the voltage U (Eq. (5)). A conventional proportional and derivative control approach is adopted, wherein K_p and K_d denote the position and velocity feedback gains, respectively. The error is defined as the deviation from the desired air-gap Δ^ss (with the superscript ss indicating steady state); U^ss represents the voltage required to achieve the desired air-gap in the equilibrium state.

Since the system stability is dictated by the vehicle-guideway interaction, it suffices to investigate the response under the moving vehicle (i.e., $\xi = 0$). To this end, the guideway response w_0 under the moving vehicle is written as follows:

$$w_0(t) = -\int_0^t G_0(t-\tau)F(\tau)\mathrm{d}\tau + w_0^{\mathrm{ic}}(t), \qquad t \geq 0, \tag{6}$$

where G_0 represents the Green's function of the guideway evaluated at $\xi = 0$ due to a moving impulse load and w_0^{ic} represents free vibrations of the guideway at $\xi = 0$ due to initial conditions corresponding to the system's equilibrium position. This term is necessary because the convolution integral captures just the response of the system with trivial initial conditions. The Green's function G_0 can be obtained from Eq. (1) by replacing F with $-\delta(t)$. By applying the Laplace transform over time, the resulting equation can be solved, expressing the Laplace-domain solution as a superposition of wave modes [4,5]. The analytical solution is then evaluated at $\xi = 0$ to determine $\hat{G}_0$ (where the hat denotes the quantity in the Laplace domain). Subsequently, its time-domain counterpart G_0 can be obtained through numerical evaluation of the inverse Laplace transform.

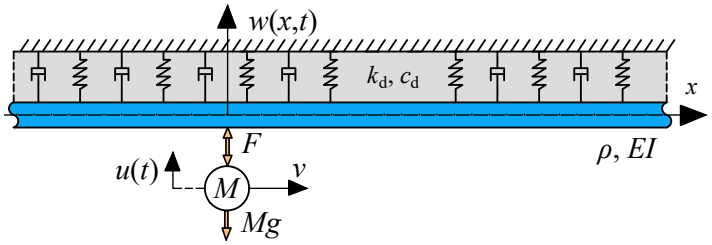

Figure 1: System representation: an infinite Euler–Bernoulli beam continuously supported by a visco-elastic foundation and subject to a moving mass. The vehicle-structure interaction is governed by the nonlinear electro-magnetic suspension.

In this study, we adopt a typical Hyperloop design previously outlined in Refs. [31,32]. Since the current model does not consider the discrete nature of the supports (see Refs. [6,9,32] for a discussion on when system periodicity should and should not be accounted for), parameters from [32] are adjusted by dividing them by the support spacing to create an equivalent distributed foundation. The vehicle is suspended from above, and the displacement w is measured at the rail level, situated at the top of the tube. Consequently, the spring stiffness in our phenomenological model not only encompasses the support stiffness but also incorporates the flexibility of the tube-rail connection and, notably, the flexibility introduced by the ovalization of the tube. Parameter values are as follows: $EI = 25\times10^6$ kNm^2, $\rho = 1400$ kg/m, $k_{\mathrm{d}} = 28\times10^3$ kN/m^2, $c_{\mathrm{d}} = 20$ kNs/m^2, $M = 7650$ kg, $C = 0.05$ Nm^2/A^2, and $\Delta^{\mathrm{ss}} = 15$ mm.

3 Linearisation of the nonlinear model

To explore the stability of the system, it is valuable to examine the linearized system around its equilibrium state. While the system described by Eqs. (2)–(6) may exhibit multiple equilibrium positions, our focus lies on the behavior around the operational equilibrium position, akin to the standard steady state of an equivalent mechanical system. To achieve this, we introduce a perturbation around the steady state by substituting $w_0(t) = w_0^{\mathrm{ss}} + w_0^{\mathrm{tr}}(t)$, $u(t) = u^{\mathrm{ss}} + u^{\mathrm{tr}}(t)$, $F(t) = F^{\mathrm{ss}} + F^{\mathrm{tr}}(t)$, and $I(t) = I^{\mathrm{ss}} + I^{\mathrm{tr}}(t)$, where the superscript *tr* denotes transient. Following mathematical manipulations, we employ the Taylor expansion to the governing equations corresponding to Eqs. (3) and (4). As a result, the linearized system is derived and expressed as follows:

$$w_0^{\mathrm{tr}} = -\int_0^t G_0(t-\tau)F^{\mathrm{tr}}(\tau)\mathrm{d}\tau, \tag{7}$$

$$M\ddot{u}^{\mathrm{tr}} = F^{\mathrm{tr}}, \tag{8}$$

$$F^{\mathrm{tr}} = \tfrac{2CI^{\mathrm{ss}2}}{\Delta^{\mathrm{ss}3}}\Big(\tfrac{\Delta^{\mathrm{ss}}}{I^{\mathrm{ss}}}I^{\mathrm{tr}} + u^{\mathrm{tr}} - w_0^{\mathrm{tr}}\Big), \tag{9}$$

$$\dot{I}^{\mathrm{tr}} = \tfrac{\Delta^{\mathrm{ss}}}{2C}\Big[-I^{\mathrm{tr}}R + K_{\mathrm{p}}\big(w_0^{\mathrm{tr}} - u^{\mathrm{tr}}\big) + \big(K_{\mathrm{d}} + \tfrac{2CI^{\mathrm{ss}}}{\Delta^{\mathrm{ss}2}}\big)\big(\dot{w}_0^{\mathrm{tr}} - \dot{u}^{\mathrm{tr}}\big)\Big], \tag{10}$$

The stability of the equilibrium state can be investigated through the eigenvalues of the linearised system. To obtain the characteristic equation, the Laplace transform is applied to Eqs. (7)–(10) with respect to time. The expression of the electro-magnetic force is substituted in the Laplace-domain counterparts of Eqs. (7) and (8), and the resulting system of equations, in matrix form, reads

$$\hat{K}_{\mathrm{dyn}}(s)\begin{pmatrix}\hat{w}^{\mathrm{tr}}\\ \hat{u}^{\mathrm{tr}}\\ \hat{I}^{\mathrm{tr}}\end{pmatrix} = \begin{pmatrix}0\\ su^{\mathrm{tr}}(t=0) + v^{\mathrm{tr}}(t=0)\\ I^{\mathrm{tr}}(t=0)\end{pmatrix}, \tag{11}$$

$$\hat{K}_{\mathrm{dyn}}(s) = \begin{pmatrix} 1-\hat{G}_0(s)\frac{2CI^{\mathrm{ss}2}}{\Delta^{\mathrm{ss}3}} & \hat{G}_0(s)\frac{2CI^{\mathrm{ss}2}}{\Delta^{\mathrm{ss}3}} & \hat{G}_0(s)\frac{2CI^{\mathrm{ss}}}{\Delta^{\mathrm{ss}2}} \\ \frac{2CI^{\mathrm{ss}2}}{\Delta^{\mathrm{ss}3}Ms^2} & 1-\frac{2CI^{\mathrm{ss}2}}{\Delta^{\mathrm{ss}3}Ms^2} & -\frac{2CI^{\mathrm{ss}}}{\Delta^{\mathrm{ss}2}Ms^2} \\ \frac{(\Delta^{\mathrm{ss}2}K_{\mathrm{d}}+2CI^{\mathrm{ss}})s+\Delta^{\mathrm{ss}2}K_{\mathrm{p}}}{-2C\Delta^{\mathrm{ss}}} & \frac{(\Delta^{\mathrm{ss}2}K_{\mathrm{d}}+2CI^{\mathrm{ss}})s+\Delta^{\mathrm{ss}2}K_{\mathrm{p}}}{2C\Delta^{\mathrm{ss}}} & \frac{\Delta^{\mathrm{ss}}R}{2C}+s \end{pmatrix},$$

where $u^{\mathrm{tr}}(t=0)$, $v^{\mathrm{tr}}(t=0)$, and $I^{\mathrm{tr}}(t=0)$ are the initial conditions of the perturbation for the mass and current. The characteristic equation is obtained by equating the determinant of the coefficient matrix to zero:

$$\left|\hat{K}_{\mathrm{dyn}}(s)\right| = 0. \tag{12}$$

It must be emphasized that the characteristic equation is neither a polynomial (since s appears also in $\hat{G}_0$ under square roots) nor a transcendental equation, meaning that it has a finite amount of roots. The eigenvalues are determined numerically by using a root finding routine (i.e., *fsolve* in Matlab) with a multitude of initial guesses for s to cover the part of the complex plane relevant for this problem.

The stability results based on the eigenvalue analysis are presented in [31] and are not repeated here since the goal of the present work is to distinguish between the two different instability mechanisms that is presented in the following.

4 Energy analysis

The eigenvalue analysis presented in the previous section is straightforward and fully describes the system's stability, but it fails to differentiate between various instability sources. Consequently, discerning the primary contributing mechanism for effective mitigation remains impossible. To judge the contribution of different components to the stability of the system, we present hereafter an investigation based the energy variation of the moving mass as done by Metrikin [23]. Because the system considered in this study is slightly different to the one in [23], the expression for the energy variation is re-derived in the following. It must be emphasized that the linearized system is used for this investigation, as was used for the eigenvalue analysis. Also, the superscript tr is omitted in the following expressions for brevity.

The variation of the moving mass energy E_{M} can be obtained by multiplying both sides of its equation of motion (Eq. (8) without superscript tr) by its velocity $\dot{u}$. Re-writing the left-hand side as $M\ddot{u}\dot{u} = \frac{\partial}{\partial t}\frac{1}{2}M\dot{u}^2$, the following expression is obtained

$$\frac{\partial}{\partial t}E_{\mathrm{M}} = F(t)\dot{u}, \qquad E_{\mathrm{M}} = \frac{1}{2}M\dot{u}^2. \tag{13}$$

The guideway contribution to the vehicle energy variation is implicitly incorporated in $F(t)$. To express it explicitly, we add and subtract the term $F(t)\dot{w}_0$ to the right-hand side of Eq. (13), thus obtaining

$$\frac{\partial}{\partial t}E_{\mathrm{M}} = \underbrace{-F(t)\dot{\Delta}}_{\text{Energy input } E_{\mathrm{em}} \text{ by electro-magnetic force}} + \underbrace{F(t)\dot{w}_0}_{\text{Energy input } E_{\mathrm{gw}} \text{ by the guideway}} \tag{14}$$

where the first term of the right-hand side represents the electro-magnetic force energy input E_{em} to the vehicle energy variation, while the second term is the guideway contribution E_{gw}. Positive input represents energy added to the mass vibration while negative input represents energy dissipation. The guideway contribution can be expressed from its equation of motion as follows [6, 33]:

$$F(t)\dot{w}_0 = -\Big[S(x,t) - vh_{\mathrm{el}}(x,t)\Big]_{x=vt-0}^{x=vt+0} + E_{\mathrm{F,h}}(t), \tag{15}$$

$$S(x,t) = EI\left(w'''\dot{w} - w''\dot{w}'\right), \qquad h_{\mathrm{el}}(x,t) = \frac{1}{2}\left[EI\left(w''\right)^2 + \rho\dot{w}^2 + k_{\mathrm{d}}w^2\right],$$

$$E_{\mathrm{F,h}}(t) = vF(t)w_0',$$

where $S(x,t)$ and $h_{\mathrm{el}}(x,t)$ represent energy flux and elastic density, respectively, and $E_{\mathrm{F,h}}(t)$ is the energy input by the horizontal force maintaining the constant vehicle velocity (for more details, see [6, 33]).

Eq. (14) shows that there are two main contributions to the energy variation of the vehicle: (i) the power input/dissipation by the electro-magnetic force, and (ii) the power input/dissipation by the guideway. Since both these contributors can cause instability, as discussed in the Introduction, they can either dissipate or input energy into the vehicle vibration. It must be emphasized that Eq. (14) (together with Eq. (15)) is the *exact* energy balance expression for the linearized system (Eqs. (7)–(10)) without any assumptions or simplifications made.

The system is unstable only if the energy variation averaged over one oscillation period is positive. Since the vibration frequency is not known apriori, the results from the eigenvalue analysis (Sect. 3) are used as input for the energy analysis performed in this section. More specifically, a harmonic motion is imposed to the mass with the frequency corresponding to the imaginary part of the eigenvalue(s) obtained in Sect. 3 and with arbitrary amplitude. The response to this system is derived in detail in [34] and is not repeated here for brevity. The averaged energy variation over one oscillation period reads

$$\Delta E_{\mathrm{M}} = \overline{E}_{\mathrm{em}} + \overline{E}_{\mathrm{gw}}, \tag{16}$$

$$\Delta E_{\mathrm{M}} = E_{\mathrm{M}}(t+T_\Omega) - E_{\mathrm{M}}(t), \qquad \overline{E}_{\mathrm{em}} = -\frac{1}{T_\Omega}\int_0^{T_\Omega} F(t)\dot{\Delta}(t)\mathrm{d}t,$$

$$\overline{E}_{\mathrm{gw}} = -\Big[\overline{S}(x) - v\overline{h}_{\mathrm{el}}(x)\Big]_-^+ + \overline{E}_{\mathrm{F,h}},$$

where the overbar indicates that the quantities have been averaged over one period $T_\Omega = \frac{2\pi}{\Omega}$ of oscillations, where Ω is the imaginary part of the eigenvalue s determined in Sect. 3.

5 Results

A negative/positive ΔE_{M} means that the free-vibration response due to a perturbation will exhibit a decay/increase with time, and this should be corroborated by the corresponding eigenvalue (from which the oscillation frequency Ω was taken) having a negative/positive real part, while $\Delta E_{\mathrm{M}} = 0$ represents the boundary between stability and instability. It may seem that the energy analysis does not bring additional information to the stability investigation since it requires the eigenvalue analysis as an input, and its output merely confirms the already known stability boundaries from the eigenvalue analysis. This is right when it comes to the stability investigation, but it does allow to determine which instability mechanism (which contributor from Eq. $\big(14\big)$) is governing.

Fig. 2 presents ΔE_{M} in the K_{p}–K_{d} parameter space for a sub-critical and a super-critical velocity. The resulting stability boundaries (i.e., curves defined by $\Delta E_{\mathrm{M}} = 0$) match perfectly the ones obtained from the eigenvalues analysis (i.e., curves defined by $\mathrm{Re}(s_n) = 0$) when instability is caused by the complex-valued eigenvalue pair (i.e., stability is lost through a Hopf bifurcation). The left instability zone, caused

by the real-valued eigenvalue being positive, is not predicted by the energy analysis because this analysis assumes a harmonic motion at the stability boundary while the left boundary is characterized by a constant rigid-body motion, not a harmonic one. Nonetheless, the stability to the right of the left boundary is correctly predicted by the energy analysis, thus demonstrating that here the system stability is indeed governed by the energy variation in Eq. (16). Furthermore, the domains where the eigenvalue analysis predicted instability (grey background) coincide with a positive ΔE_{M}, which further confirms the validity of the energy analysis.

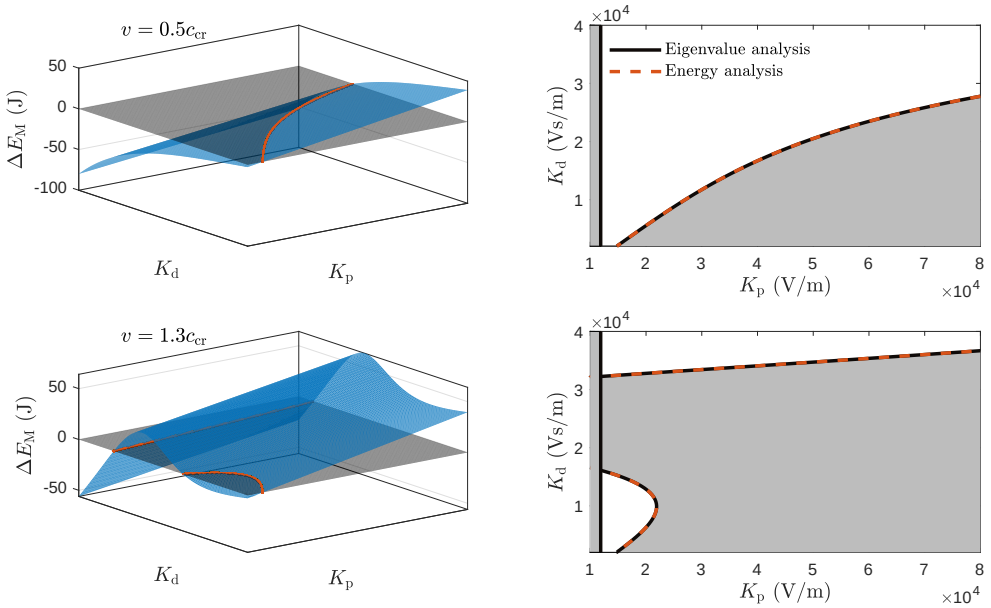

Figure 2: ΔE_{M} (left panels) and $\Delta E_{\mathrm{M}} = 0$ (right panels) in the K_{p}–K_{d} parameters space for two vehicle velocities: $v = 0.5c_{\mathrm{cr}}$ (top panels) and $v = 1.3c_{\mathrm{cr}}$ (bottom panels). The curves defined by $\mathrm{Re}(s_n) = 0$ from the eigenvalue analysis are superimposed in the right panels.

Taking advantage of the energy analysis, Fig. 3 presents the separate contribution of the electro-magnetic and wave-induced instability mechanisms. The contributions are presented along the K_{d} axis for one selected value of K_{p} (their 3-D representation in the K_{p}–K_{d} parameter space was considered unclear by the authors). To emphasize the influence of the guideway, the curve describing zero energy input by the electro-magnetic force (i.e., $\overline{E}_{\mathrm{em}} = 0$) is also presented; this curve represents the stability boundary when the guideway is considered as rigid [17, 18, 35].

On the one hand, the results for $v = 0.5c_{\mathrm{cr}}$ (Fig. 3) demonstrate that the instability at sub-critical velocities is caused by the electro-magnetic force having a positive energy input ($\overline{E}_{\mathrm{em}} > 0$). The guideway, through its negative energy input (i.e., energy dissipation), proves to be a stabilizing mechanism and, consequently, enlarges the stability domain ($\overline{E}_{\mathrm{em}} = 0$ curve is the reference in which the guideway is not accounted for). On the other hand, the results for $v = 1.3c_{\mathrm{cr}}$ show that, for a range of K_{d}, $\overline{E}_{\mathrm{gw}}$ is positive and is the main cause of instability at super-critical velocities, while

$\overline{E}_{\mathrm{em}}$ is mainly negative, thus being a stabilizing mechanism. Fig. 3 demonstrates the complex interaction between the electro-magnetic and wave-induced instability, where each one can be a stabilizing or destabilizing mechanism depending on the vehicle velocity.

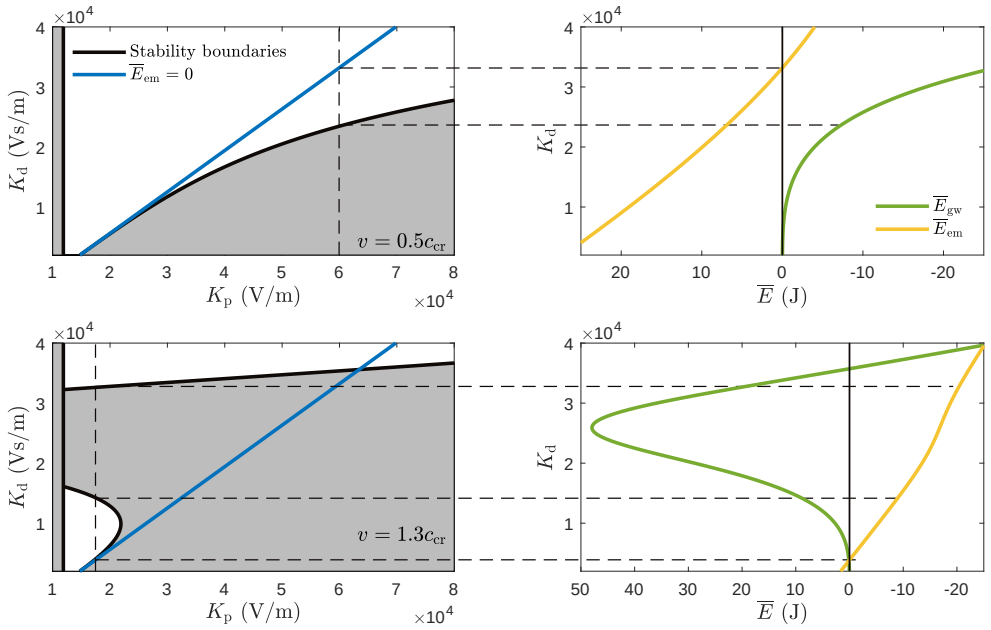

Figure 3: Left panels: Stable/unstable domains in the K_{p}–K_{d} parameter space and the curve corresponding to no energy input by the electro-magnetic force (i.e., $\overline{E}_{\mathrm{em}} = 0$). Right panels: energy input by the electro-magnetic force $\overline{E}_{\mathrm{em}}$ and by the guideway $\overline{E}_{\mathrm{gw}}$ vs K_{d} for one value of K_{p} indicated by the vertical dashed black line in the left panels. These results are presented for two vehicle velocities: $v = 0.5c_{\mathrm{cr}}$ (top panels) and $v = 1.3c_{\mathrm{cr}}$ (bottom panels).

6 Concluding remarks

The authors have previously investigated [31] the unstable velocity regimes of the Hyperloop vehicle-structure interaction and their dependency on the control gains by properly accounting for the frequency and velocity dependent reaction force provided by the infinite guideway. Furthermore, that study focused on the interplay between two fundamentally different instability sources, namely (i) the electro-magnetic suspension, and (ii) wave-induced instability, showing that stability domains drastically change above a certain vehicle velocity. The current study presented a methodology to distinguish the contribution of each instability mechanism to the overall system stability.

To discern the individual contributions, the energy variation of the vehicle is divided in two components corresponding to (i) energy input by the electro-magnetic

suspension and (ii) energy input by the guideway. The results obtained through the energy analysis are validated against the ones previously obtained using an eigenvalue analysis. The results of the energy analysis show that at low relative velocities, the electro-magnetic suspension can be destabilizing for certain control gains while the guideway is stabilizing for any control gains. At large relative velocities, the main destabilizing mechanism is the guideway while the electro-magnetic suspension can be either stabilizing or destabilizing depending on the control gains. The energy analysis demonstrates the complex interaction between the electro-magnetic and wave-induced instability, where each one can be a stabilizing or destabilizing mechanism depending on the vehicle velocity and control gains.

While identifying unstable velocity regimes is practical for Hyperloop design, the ability to discern which mechanism causes system instability for a certain parameter combination is valuable can be crucial for efficient mitigation. This investigation offers physical insight into the mechanisms that can cause instability in the Maglev/Hyperloop systems, and can help engineers that develop this novel transportation system to avoid excessive vibrations and, in extreme cases, derailment.

References

[1] Dan Stăncioiu, Huajiang Ouyang, and John E. Mottershead. Vibration of a beam excited by a moving oscillator considering separation and reattachment. *Journal of Sound and Vibration*, 310(4-5):1128–1140, 2008.

[2] Traian Mazilu. Instability of a train of oscillators moving along a beam on a viscoelastic foundation. *Journal of Sound and Vibration*, 332(19):4597–4619, 2013.

[3] Nicholas A. Alexander and Mohammad M. Kashani. Exploring Bridge Dynamics for Ultra-high-speed, Hyperloop, Trains. *Structures*, 14:69–74, jun 2018.

[4] Andrei B. Fărăgău, Andrei V. Metrikine, and Karel N. van Dalen. Transition radiation in a piecewise-linear and infinite one-dimensional structure–a Laplace transform method. *Nonlinear Dynamics*, 98:2435–2461, 2019.

[5] Andrei B. Fărăgău, Traian Mazilu, Andrei V. Metrikine, Tao Lu, and Karel N. van Dalen. Transition radiation in an infinite one-dimensional structure interacting with a moving oscillator—the Green's function method. *Journal of Sound and Vibration*, 492:115804, 2021.

[6] Andrei B. Fărăgău. *Understanding degradation mechanisms at railway transition zones using phenomenological models*. PhD thesis, Delft University of Technology, 2023.

[7] João Manuel de Oliveira Barbosa, Andrei B. Fărăgău, and Karel N. van Dalen. A lattice model for transition zones in ballasted railway tracks. *Journal of Sound and Vibration*, 494(November):115840, 2021.

[8] João Manuel de Oliveira Barbosa, Andrei B. Fărăgău, Karel N. van Dalen, and Michael Steenbergen. Modelling ballast via a non-linear lattice to assess its compaction behaviour at railway transition zones. *Journal of Sound and Vibration*, 530(April):116942, 2022.

[9] Andrei B. Fărăgău, João M. de Oliveira Barbosa, Andrei V. Metrikine, and Karel N. van Dalen. Dynamic amplification in a periodic structure with a transition zone subject to a moving load: three different phenomena. *Mathematics and Mechanics of Solids*, 27(9):1740–1760, 2022.

[10] A. V. Metrikine. Parametric instability of a moving particle on a periodically supported infinitely long string. *Journal of Applied Mechanics, Transactions ASME*, 75(1):0110061–0110068, 2008.

[11] S. N. Verichev and A. V. Metrikine. Instability of vibrations of a mass that moves uniformly along a beam on a periodically inhomogeneous foundation. *Journal of Sound and Vibration*, 260(5):901–925, 2003.

[12] Kazuhisa Abe, Yuusuke Chida, Pher Errol Balde Quinay, and Kazuhiro Koro. Dynamic instability of a wheel moving on a discretely supported infinite rail. *Journal of Sound and Vibration*, 333(15):3413–3427, 2014.

[13] Hyung Woo Lee, Ki Chan Kim, and Ju Lee. Review of Maglev train technologies, jul 2006.

[14] Donald M. Rote and Yigang Cai. A review of dynamic stability of repulsive-force Maglev suspension systems. *IEEE Transactions on Industrial Electronics*, 38(2):1383–1390, 2002.

[15] Ahmed S. Abdelrahman, Jawwad Sayeed, and Mohamed Z. Youssef. Hyperloop Transportation System: Analysis, Design, Control, and Implementation. *IEEE Transactions on Industrial Electronics*, 65(9):7427–7436, 2018.

[16] Junxiong Hu, Weihua Ma, Xiaohao Chen, and Shihui Luo. Levitation Stability and Hopf Bifurcation of EMS Maglev Trains. *Mathematical Problems in Engineering*, 2020, 2020.

[17] Jithu Paul, Andrei B. Fărăgău, Rens J. van Leijden, Andrei V. Metrikine, and Karel N. van Dalen. The stability behaviour of an electromagnetically suspended Hyperloop vehicle subject to aeroelastic forcing. In *Railway2024 Conference Proceedings*, 2024.

[18] Han Wu, Xiao Hui Zeng, Ding Gang Gao, and Jiang Lai. Dynamic stability of an electromagnetic suspension maglev vehicle under steady aerodynamic load. *Applied Mathematical Modelling*, 97:483–500, 2021.

[19] Hiroshi Yabuno, Takehisa Seino, Masatsugu Yoshizawa, and Yasushi Tsujioka. Dynamical behaviour of a levitated body with magnetic guides. *JSME International Journal*, 32(3):428–435, 1989.

[20] Konstantinos Gkoumas. Hyperloop academic research: A systematic review and a taxonomy of issues. *Applied Sciences (Switzerland)*, 11(13), 2021.

[21] Pedro Museros, Carlos Lázaro, Benjamín Pinazo, and Salvador Monleón. Key aspects in the analysis and design of Hyperloop™ infrastructure under static, dynamic and thermal loads. *Engineering Structures*, 239(April), 2021.

[22] G. G. Denisov, E. K. Kugusheva, and V. V. Novikov. On the problem of the stability of one-dimensional unbounded elastic systems. *Journal of Applied Mathematics and Mechanics*, 49(4):533–537, 1985.

[23] Metrikin A.V. Unstable vertical oscillations of an object moving uniformly along an elastic guide as a result of an anomalous Doppler effect. *Acoustical Physics*, 40(1):85–89, 1994.

[24] R. Bogacz, S. Nowakowski, and K. Popp. On the Stability of a Timoshenko Beam on an Elastic Foundation Under a Moving Spring-Mass System. *Acta Mechanica*, 61:117–127, 1986.

[25] A. V. Metrikine and K. Popp. Instability of vibrations of an oscillator moving along a beam on an elastic half-space. *European Journal of Mechanics, A/Solids*, 18(2):331–349, 1999.

[26] Stanislav Nikolaevich Veritchev. *Instability of a vehicle moving on an elastic structure*. PhD thesis, Delft University of Technology, 2002.

[27] Traian Mazilu, Mădălina Dumitriu, and Cristina Tudorache. Instability of an oscillator moving along a Timoshenko beam on viscoelastic foundation. *Nonlinear Dynamics*, 67(2):1273–1293, 2012.

[28] C. Rodrigues, F. M. F. Simões, A. Pinto da Costa, D. Froio, and E. Rizzi. Finite element dynamic analysis of beams on nonlinear elastic foundations under a moving oscillator. *European Journal of Mechanics, A/Solids*, 68(October 2017):9–24, 2018.

[29] Mingjuan Zhao, João Manuel de Oliveira Barbosa, Jun Yuan, Andrei V. Metrikine, and Karel N. van Dalen. Instability of vibrations of an oscillator moving at high speed through a tunnel embedded in soft soil. *Journal of Sound and Vibration*, 494:115776, 2021.

[30] Zuzana Dimitrovová. On the Critical Velocity of Moving Force and Instability of Moving Mass in Layered Railway Track Models by Semi-analytical Approaches. *Vibration*, 6(1):113–146, 2023.

[31] Andrei B. Fărăgău, Rui Wang, Andrei V Metrikine, and Karel N Van Dalen. The interplay between the electro-magnetic and wave-induced instability mechanisms in the Hyperloop transportation system. In *Nodycon2023 Proceedings*, 2023.

[32] Andrei B. Fărăgău, Andrei V. Metrikine, and Karel N. van Dalen. Dynamic amplification in a periodic structure subject to a moving load passing a transition zone: Hyperloop case study. In *Recent Trends in Wave Mechanics and Vibrations*, 2022.

[33] A. I. Vesnitskii and A. V. Metrikin. Transition radiation in mechanics. *Physics-Uspekhi*, 39(10):983–1007, 1996.

[34] Andrei B. Fărăgău, Andrei V. Metrikine, Jithu Paul, Rens van Leijden, and Karel N. van Dalen. The interaction between the electro-magnetic and wave-induced instability mechanisms in magnetically-levitated transportation systems. *Journal of Sound and Vibration (in review process)*, 2024.

[35] Renato Galluzzi, Salvatore Circosta, Nicola Amati, Andrea Tonoli, Angelo Bonfitto, Torbjörn A. Lembke, and Milan Kertész. A Multi-domain Approach to the Stabilization of Electrodynamic Levitation Systems. *Journal of Vibration and Acoustics, Transactions of the ASME*, 142(6):1–30, 2020.